remote sensing

MDPI

Article

Mapping Live Coral: Comparing Spaceborne to Airborne Imaging Spectroscopy

Gregory P. Asner [1,2,3,*], Nicholas R. Vaughn [1], Joseph Heckler [1], Keely L. Roth [4] and Amy Rosenthal [4]

[1] Center for Global Discovery and Conservation Science, Arizona State University, Hilo, HI 96720, USA; nickvaughn@asu.edu (N.R.V.); joseph.heckler@asu.edu (J.H.)
[2] School of Ocean Futures, Arizona State University, Hilo, HI 96720, USA
[3] School of Geographic Sciences and Urban Planning, Arizona State University, Tempe, AZ 85281, USA
[4] Planet Labs PBC, San Francisco, CA 94107, USA; keely.roth@planet.com (K.L.R.); amy.rosenthal@planet.com (A.R.)
* Correspondence: gregasner@asu.edu

Highlights

What are the main findings?

- Spaceborne imaging spectroscopy from the Tanager-1 satellite provided verifiable estimates of live coral cover on a Hawaiian reef.
- Airborne and spaceborne imaging spectrometers produced comparable geospatial distributions of live coral cover, macroalgal cover, and their ratio.

What are the implications of the main findings?

- Live coral cover can be mapped with high-fidelity imaging spectroscopy from Earth orbit.
- The findings support repeatable mapping of coral and macroalgae in reef compositional monitoring at a global scale.

Abstract

Live coral cover is a key indicator of coral reef composition, health, and functioning. Airborne imaging spectroscopy provides verifiably accurate estimates of live coral cover to seawater depths of 25 m, yet satellite-based approaches have not achieved the same level of performance. The new Tanager-1 satellite carries a high-fidelity imaging spectrometer in sun-synchronous Earth orbit, providing an opportunity to transition from airborne to spaceborne imaging of live corals and other benthic constituents. We coordinated overpasses of Tanager-1 and Global Airborne Observatory (GAO) imaging spectrometer measurements of coral reef to a depth of 25 m in Hawai'i. Tanager-1 has a spatial resolution of 30 m, while the GAO data were collected at 2 m resolution, requiring detailed modeling to simulate 30 m data for subsequent comparison to the satellite data. At 30 m resolution, the two sensors generated similar geographic patterns of live coral, macroalgal, and sand cover. Field validation indicated similar precision and accuracy of live coral cover estimates, and the ratio of live coral to macroalgal cover proved similar between sensors. Overall results indicate that live coral cover can be mapped with high-fidelity imaging spectroscopy from Earth orbit. With the advent of more spaceborne imaging spectrometers, a new era of live coral monitoring will be possible, filling a critical gap for repeated assessments of reef compositional change at a global level.

Keywords: coral reef; Global Airborne Observatory; Hawai'i; hyperspectral; Tanager

Check for updates

Academic Editor: Raphael M. Kudela

Received: 15 December 2025
Revised: 27 January 2026
Accepted: 28 January 2026
Published: 29 January 2026

Copyright: © 2026 by the authors. Licensee MDPI, Basel, Switzerland. This article is an open access article distributed under the terms and conditions of the Creative Commons Attribution (CC BY) license.

1. Introduction

Live coral cover, denoting the proportion of the seafloor occupied by living coral tissue, is a fundamental indicator of coral reef condition. Compared to the prevalent utilization of diver-based surveys in small-scale reef assessments of live coral cover, satellite remote sensing has offered relatively limited coral information at reef to global scales. Multispectral satellite sensors, including Landsat [1], Planet Dove [2,3], IKONOS [4], WorldView-2/3 [5], and Sentinel-2 [6,7], have been successfully utilized in the mapping of benthic habitat, geomorphological features, and reef-scale coral bleaching events. However, a very limited number of satellite-based studies have attempted to retrieve the percentage of live coral cover within reefs. While IKONOS and Worldview-2 have been used to estimate live coral cover [5,8–12], satellite-derived estimates remain rare and unverified due to spectral confusion between live coral, macroalgae, sand and rubble, which is made much more challenging by seawater attenuation [6,13]. Many multispectral satellite sensors lack the spectral resolution required to discriminate live coral from other benthic constituents at increasing seawater depths [14–16]. As a result, global satellite-based maps of live coral cover have not yet emerged [17,18].

While satellite-based multispectral approaches remain limited for detecting and mapping live corals, airborne imaging spectrometers have demonstrated their capability in detecting and separating live coral from other benthic constituents. Compact Airborne Spectrographic Imager (CASI) data were used to map live coral with demonstrable accuracy [19,20]. Airborne Visible and Infrared Imaging Spectrometer (AVIRIS) imagery was successfully analyzed into benthic constituents including live coral, algae, and sand [21]. The Global Airborne Observatory (GAO; formerly Carnegie Airborne Observatory; [22]) has operationally mapped live coral cover at archipelago scales using a high-fidelity imaging spectrometer [23,24]. In addition, drone and underwater vehicle-mounted hyperspectral sensors have enabled centimeter-resolution coral mapping over smaller areas [25,26]. A few spaceborne imaging spectrometers, such as NASA's Earth Observing-1 Hyperion and Germany's EnMAP, have been used for substrate classification or coral bleaching detection (e.g., [27]), but none have produced verifiable data on live coral cover.

While the potential for live coral mapping from spaceborne imaging spectroscopy has existed for more than a decade, there have been few opportunities to compare and contrast new satellite and established airborne approaches using this technique. In 2024, Planet Labs PBC launched the Tanager-1 satellite carrying a high-fidelity imaging spectrometer to low Earth orbit (hereafter referred to as Tanager). The instrument onboard Tanager is a close technological derivative of the AVIRIS and GAO Visible-to-Infrared Imaging Spectrometers [28], but coordinated overpasses of Tanager with AVIRIS and/or GAO have not been possible for comparative assessments of performance in natural resource mapping.

Here we sought to coordinate data collections from Tanager and the GAO to assess the potential for live coral cover determination using spaceborne imaging spectroscopy data. The GAO live coral maps had been validated in past studies [23,24], indicating high accuracy (R^2 = 0.94) and high precision (root mean squared error [RMSE] of 7.7% cover) relative to field plot data at 2 m resolution using a deep learning network analysis framework. In the present study, we employed a more general nearest neighbor analytical technique to compare and contrast Tanager and GAO estimates of live coral cover along 50.3 km of coastline off the island of Hawai'i. Because the GAO provided a 2 m spatial resolution product, while Tanager provided a 30 m spatial resolution product, we used detailed instrument and atmospheric modeling to generate a valid comparison between the two imaging systems and their resulting reef products.

2. Materials and Methods

2.1. Study Region

GAO and Tanager imaging spectrometer data were acquired in January 2025 along the northwest coastline of Hawai'i Island, USA. This area was covered in a single overpass of the Tanager satellite (Figure 1). Within this region, reef composition ranges from algal-dominated with minimal live coral to areas of extensive live coral cover [24,29]. In addition, there are multiple large stream outlets with a significant amount of sediment input into embayments, as well as seasonal ocean swell events that result in a variety of turbid water conditions throughout the year. These characteristics provided a complex test environment within which to compare live coral mapping abilities of these two sensors.

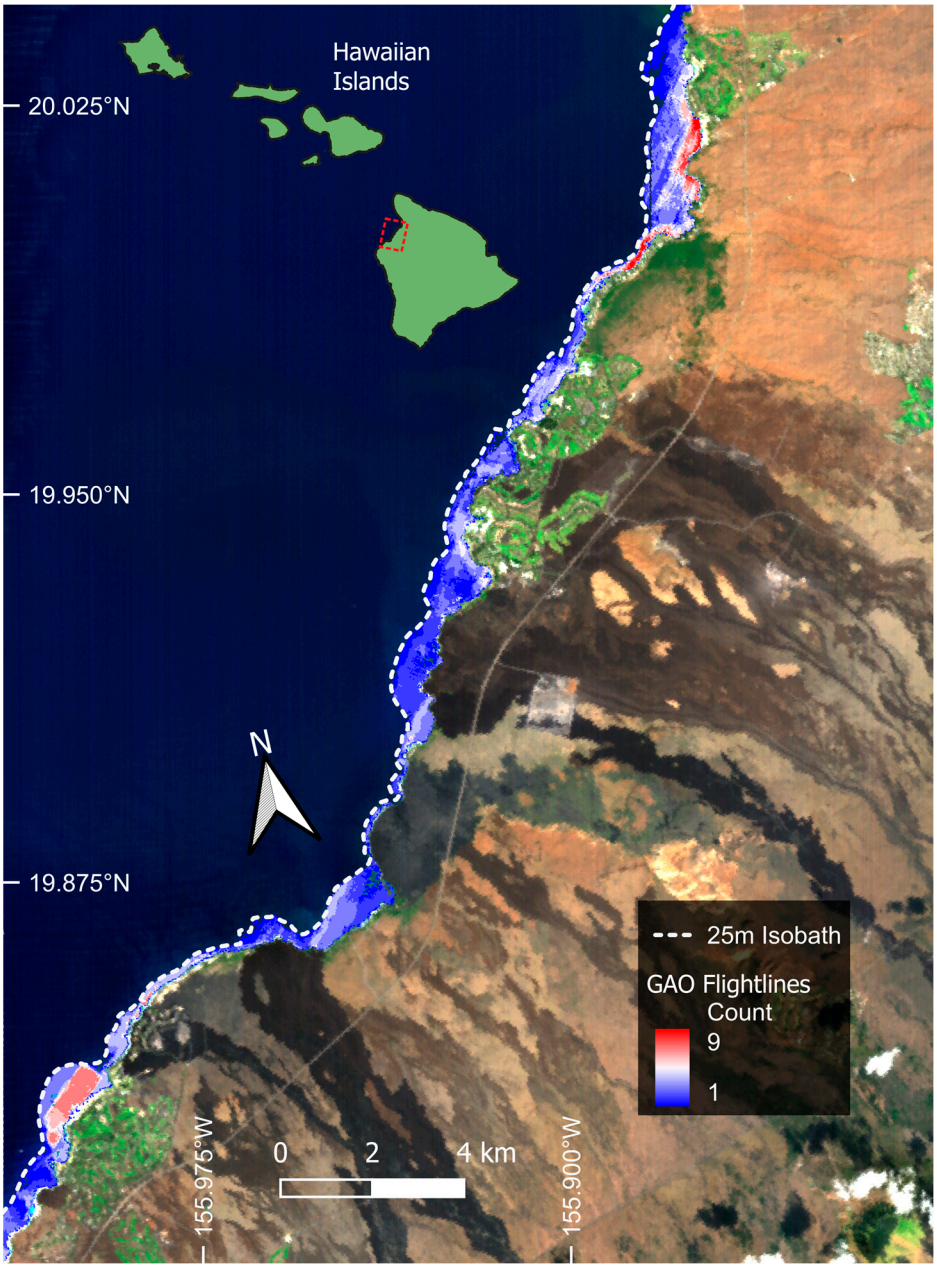


Figure 1. The study region of interest imaged using the Tanager satellite, displayed as a natural color composite image. The dashed white line delineates the reef extent to 25 m water depth. The number of Global Airborne Observatory (GAO) flight lines collected during the January 2025 campaign are shown with a blue-to-red coloring. The location of the study within the State of Hawai'i is shown in the red dashed box in the upper left.

2.2. Satellite Imagery

To evaluate the benthic mapping performance of the Tanager spectrometer, we used a single contiguous dataset collected on 24 January 2025 at 11:25 am local time (Figure 1). The imagery was downloaded directly from the source using the Application Programming Interface provided by Planet Labs PBC (San Francisco, CA, USA). The imagery on this date was free of cloud and cloud shadow over the reef and coastal region, and it had minimal sea surface glint. This time of day is ideal for mapping benthic cover because the sun angle is high enough to limit shadowing within the 3-dimensional structure of the reef, yet low enough to reduce the glint reflected back at the sensor. The Tanager imagery was collected in "standard sensitivity" mode with an integration time of 8 ms. Radiance data were composed of 424 spectral bands, each with approximately 5 nm band center spacing (5.4–6.8 nm full width at half maximum, FWHM), across a wavelength range of 376–2489 nm.

We processed the raw radiance spectra to hemispherical-directional surface reflectance using the apply_oe tool available in the ISOFIT package version 3.5.1 [30,31]. We parameterized ISOFIT using the surface model configuration version 20240103 and spectral libraries from the NASA EMIT mission L2 data processing algorithm [32,33]. Observation angles necessary for atmospheric correction as well as latitude and longitude ground coordinates for all pixels were obtained from the HDF5-formatted radiance dataset, and elevations were interpolated at these pixel locations from the Copernicus COP-30 30 m global elevation map [34]. The apply_oe tool was configured to initially run full atmospheric parameter estimation on superpixel clusters of 53 pixels (approx. 4.8 ha), then apply the "analytical line" method to derive optimal reflectance values for each pixel with the interpolated atmospheric properties fixed. These surface reflectance spectra, $\rho_w(\lambda)$, that were output by the atmospheric correction workflow were converted to remote sensing reflectance in sr^{-1} units, $R_{rs}(\lambda)$, required for our benthic mapping algorithms, by dividing the spectra by π.

We previously tested these ISOFIT settings on GAO data collected simultaneously with in situ field spectrometer measurements [35] (Figure 2). In that study, we compared the processed GAO R_{rs} spectra against R_{rs} field measurements made using a handheld SVC HR-512i spectroradiometer (Spectra Vista Corporation, Pughkeepsie, NY USA) while following the protocols of the International Ocean Color Coordinating Group (IOCCG) [36]. In this comparison, we found that the ISOFIT methodology described above is sufficient to retrieve accurate surface reflectance reading from the GAO sensor for the purposes of benthic mapping.

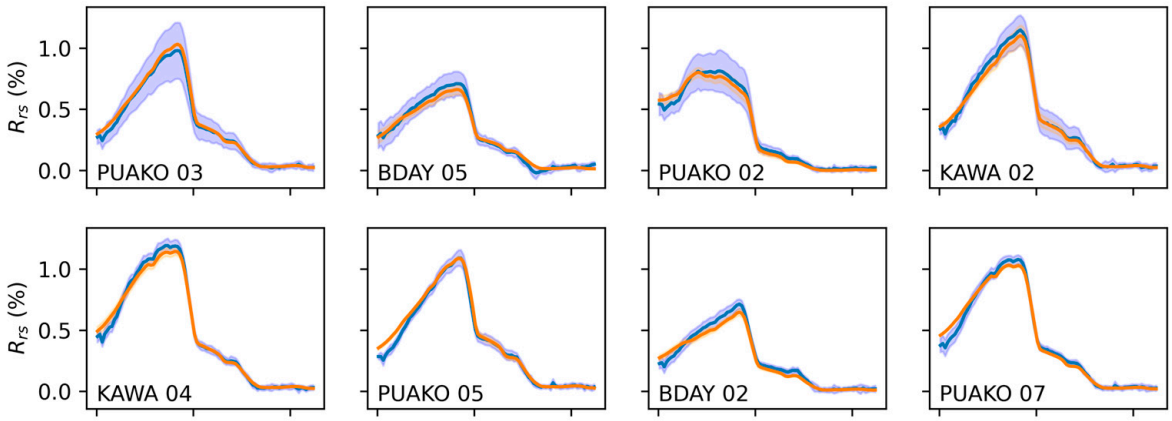


Figure 2. *Cont.*

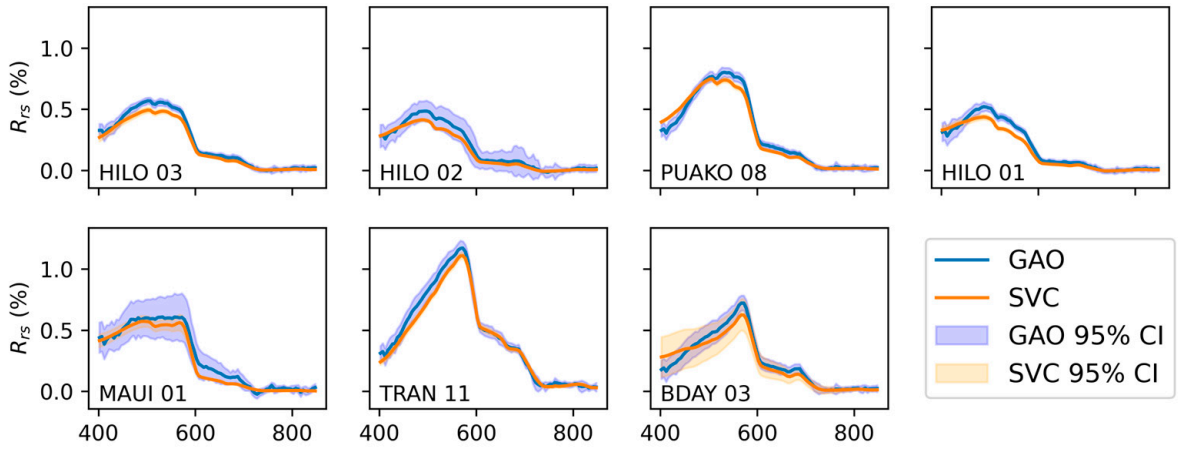


Figure 2. Demonstration that the ISOFIT apply_oe tool, using the settings and parameterization used in this study, can successfully model the atmosphere and retrieve water surface reflectance (ρ_w). Each panel represents a paired SVC field spectrometer reading of remote sensing reflectance (R_{rs}, as ρ_w / π) with simultaneously collected GAO spectroscopy from the Hawaiian islands. Spectra from both instruments have had glint removed using the 4C model [37].

2.3. GAO Imagery

A GAO mapping campaign took place in January 2025 to coincide with the Tanager satellite data collection period (Figure 1). The GAO flew the western Hawaii Island coastline daily to create a mosaic with varying sun-sensor, water quality and sea surface conditions. Each of the GAO data collections took place from 0900 to 1130 h, compiling a total of 32 flight lines throughout the study region collected from 11 to 16 January 2025.

To compare the performance of Tanager to GAO, we processed each GAO flight line covering reef to a depth of 25 m. Because the native spatial resolution of the GAO imagery from this campaign is much finer than the Tanager imagery, we processed the GAO imagery at both a 2 m resolution and a resampled 30 m resolution to assess the impact of spatial resolution on the results and to provide a comparison between the satellite and airborne sensors. Resampling to 30 m was carried out by first averaging the image geometry model (IGM) array, which contains the UTM zone 5 Northing and Easting locations of the original 2 m GAO data, on a 15 pixel × 15 pixel grid in the raw sampling space to obtain the pixel center locations matching a 30 m grid. Next, we computed distance-weighted averages of the GAO radiance data at these grid centers using a 2-dimensional Gaussian kernel to simulate the point spread function of the Tanager sensor. We then computed the standard deviation (σ) of this kernel (Equation (1)). All pixels within a 2σ radius neighborhood of each 15 pixel × 15 pixel grid center location were assigned a weight based on their Euclidean distance to this center in UTM coordinates and the weighted average of the full radiance spectrum was computed. These average GAO spectra (containing 428 bands covering 348–2486 nm with FWHM values of 5.49–5.82 nm) were interpolated to the same band centers and FWHM of Tanager using integrations of Gaussian response functions with specified FWHM values.

$$\sigma = \frac{30}{2\sqrt{2\ln(2)}} \quad (1)$$

The resampled GAO radiance spectra were smoother than the Tanager spectra because sampling noise was effectively averaged out. To make the resampled GAO data more comparable to Tanager, and to assess the influence of such noise in mapping results, we added random noise back into the 30 m GAO spectra using a radiometric model provided by Planet Labs that defines distributions for multiple sources of noise during a standard 8 ms Tanager image collection [28]. For each pixel for each of three permutations of resampled

30 m GAO data, we drew random values from these noise distributions to be added to the resampled spectrum. With the noise-added resampled 30 m GAO flight line radiance data, we used the same atmospheric correction as for Tanager to estimate surface reflectance in each 30 m pixel.

2.4. Inter-Sensor Reflectance Calibration

During initial comparison between the sensors, we found that the Tanager reflectance spectra brighter than those of the GAO in the blue end of the spectrum. We found that this difference declined smoothly along an approximately exponential decline from 0.005 sr^{-1} at 400 nm to no difference at 800 nm (Figure 3). This bias was found to consistent over both land and water surfaces across multiple Tanager images—we had access to several images that were not used in this project due to clouds and/or glint—and for multiple years of GAO coverage. Additionally, the bias was unaffected by pixel brightness (Figure 3). This consistency of the bias across time, target, and our inability to affect bias through multiple iterations of changing the atmospheric correction parameters all point to a need for a radiance calibration adjustment for the Tanager sensor.

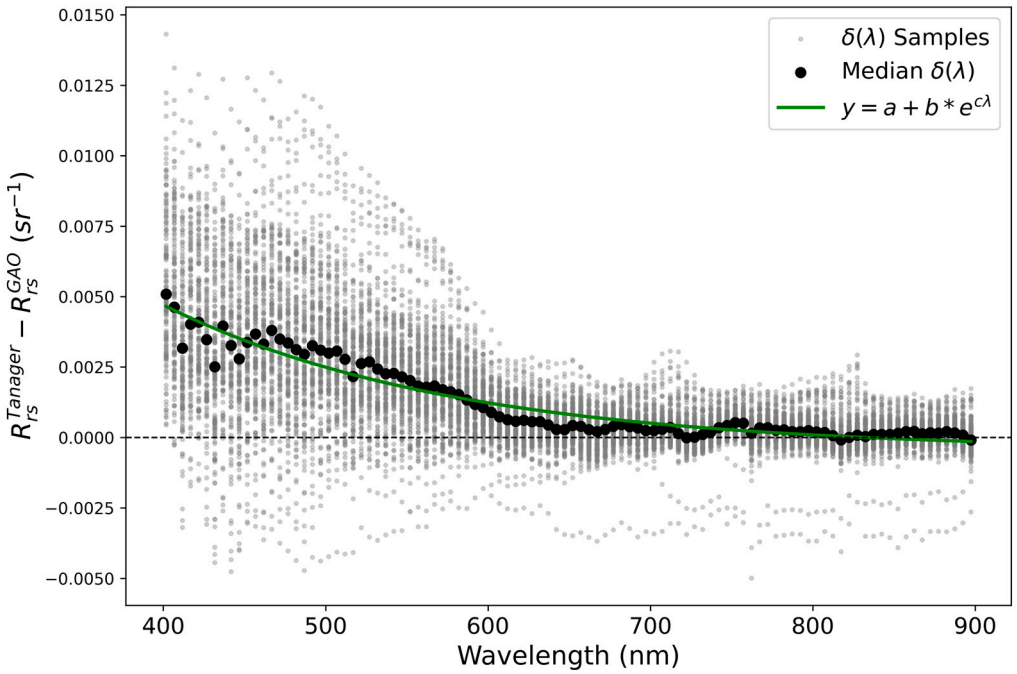


Figure 3. Representation of the bias between Tanager remote sensing reflectance and that of the GAO for 30 randomly selected water points in the overlap of both datasets. Each gray point represents the bias, $\delta(\lambda)$, of Tanager from one GAO flight line at one the 30 points at a given wavelength. The larger black points represent the median bias across all the gray points. The green line is an exponential fit between the medians for each band.

Thought the bias was too minimal to really be noticeable when working with bright land pixels, we found that the bias in dark water spectra affected the water masking and models described below. To overcome this we treated the measured bias as a constant spectral function and removed it from the Tanager reflectance data. This was done by computing the average difference between GAO and Tanager reflectance between over a uniform dark volcanic lava surface located along the coastline within the coaligned imagery and subtracting this spectral-valued difference from the Tanager reflectance data.

2.5. Water and Depth Masking

For each reflectance image, we generated a mask to isolate pixels in the 0–25 m depth range over the reef. Pixels containing water had to pass a series of spectral detection thresholds to delineate well-lit, smooth surface water from shadow or white water and terrestrial targets. Any pixel failing one or more of the following checks of water reflectance was removed from subsequent analyses:

1. An Automated Water Extraction Index [38], computed as

$$AWEI = 4\ (R_{560} - R_{1650}) - (0.25\ R_{830} + 2.75\ R_{2215}),$$

greater than −0.05;

2. A Modified Normalized Difference Water Index [39], computed as

$$MNDWI = (R_{559} - R_{1240})\ /\ (R_{559} + R_{1240}),$$

greater than 0.25;

3. A near-infrared glint metric, computed as the mean reflectance of all bands between 880 and 920 nm, less than 0.15;
4. A brightness metric, computed as the mean reflectance of all bands between 500 and 560 nm, greater than 0.015;
5. Either:
    a. The same brightness metric as in (4) above less than 0.15;
    b. A blue-green slope index, computed as

$$BGSI = (R_{490} - R_{440})\ /\ R_{440},$$

greater than 0.01,

where R_w refers to the reflectance value in the band with center wavelength nearest to wavelength w, in nanometers (nm).

Depth was masked using a coastline model originally derived at 2 m resolution [29]. For 30 m processing, this map was resampled using a simple averaging filter, and a mask was generated for pixels above 25 m depth. The depth and water masks were combined into a single mask of invalid pixels and applied to the reflectance data.

2.6. Benthic Cover Estimation

Our previous work [23,24] incorporated the use of deep learning (DL) network models. These DL models are extremely accurate, but despite using tactics to reduce overfitting, they were highly tuned to features of the GAO instrument spectra used in training them and therefore not transferable to new imaging data sets. When we attempted to apply these DL models to new data collected in subsequent years, we found that a new model needed to be trained for each new imaging dataset, reducing model generalizability and applicability to new imaging spectroscopy datasets. Training separate models for GAO and Tanager data adds another source of error that would confound any conclusions that might be made about the mapping capability of the GAO and Tanager instruments.

In recent work (G. Asner and N. Vaughn, unpub. data), we found that using simulated surface reflectance spectra for model training, while less accurate for any individual image dataset, proved far more stable and transferrable across image datasets because the model cannot overfit to the measured reflectance data. Therefore, in this study we estimated benthic cover of live coral, macroalgae, sand, and bare rock using a k-nearest neighbor (K-NN) machine learning approach to match observed reflectance to a library of simulated reference surface reflectance spectra. This library was created using an aquatic radiative transfer model-bio_optics-with components for modeling the

optical properties of water as well as sun and sky glint [36,40,41]. To create this library, we incorporated four libraries of bottom reflectance spectra previously collected with handheld underwater spectrometers [15].

For each of 2.5 million iterations, we used a bottom reflectance model created as the linear sum of per-class fractional cover and a random set of four benthic spectra—one sample drawn from each class. Fractional cover values were also randomly selected but were constrained so that the four values summed to one for each iteration. Next, we used the bio_optics model to simulate the forward propagation of reflected light through a medium of water with optical properties defined by random values of depth as well as amounts of fine and coarse particles (mg L^{-1}), phytoplankton (µg L^{-1}), and colored dissolved organic matter (CDOM; L^{-1}) randomly drawn from a specified uniform (depth) or beta (others) distribution. The absorption spectra of phytoplankton and CDOM are themselves generated from a linear combination of user-specified libraries based on field sampling [36,40]. After transfer through the water column, contributions of sun and sky glint were also defined using a 5-parameter model to simulate the spectral shape and magnitude of glint input to the modeled surface reflectance [36,41]. After resampling the simulated spectra to match the wavelengths of the input reflectance spectra, the benthic and water properties for every valid GAO and Tanager reflectance pixel were estimated using an average of the associated values for the five nearest simulated spectra using Euclidean distance and limited to the fitting window of 410–720 nm. The model estimates represent the relative influence of live coral cover on measured surface reflectance, and these values were found to have a non-linear relationship with values of fractional cover of live coral as measured in the field, likely due to the 3-dimensional structure of coral colonies and other constituents in the scene. During validation of this approach in other work, we found that this relationship could be mapped using a smoothing spline model of field-derived cover estimates and that the benthic cover estimates could be adjusted to fractional cover values using the inverse of this spline function (G. Asner and N. Vaughn, unpub. data).

We compared the fractional cover estimates from the Tanager imagery to those of the GAO imagery by assessing whether differences were within the range of variation we observed across the various GAO flight lines over the same locations. For this we computed a 95% confidence interval (CI) as mean $\pm$ 1.96 times the standard deviation within a 3 pixel $\times$ 3 pixel moving window for each 30 m $\times$ 30 m pixel within the study region. The mean and standard deviations for these CIs were the sample average and standard deviation of the cover fractional cover across all GAO flight lines and noise permutations of these flight lines covering the given pixel for each of the live coral, macroalgae, and sand classes.

2.7. Orthorectification

Benthic cover maps resulting from the above steps were still in the original row and column space as collected by the spectrometer instruments, and these data needed to be orthorectified so they could be presented as spatial maps and compared to field data. For this we converted the IGM pixel locations to geographic lookup tables (GLT) by creating a pixel grid at the associated spatial resolution (2 m or 30 m). For each pixel in these GLTs, we determined the IGM pixel nearest to the GLT pixel center location in UTM coordinates and then stored the row and column address of this IGM pixel within the GLT file. Orthorectified maps of benthic cover could then be made by building the same pixel grid as represented in the GLT and transferring the benthic cover data at the row and column locations stored in the GLT. This was done for the single Tanager scene as well as separately for each of the 31 GAO flight lines covering the study area. For comparison purposes, the following benthic cover datasets were created (Table 1):

Table 1. Summary of Global Airborne Observatory (GAO) and Tanager data sets generated and tested in this study.

GAO 2 m	2 m resolution maps produced by applying the model to native resolution GAO reflectance imagery;
GAO 2 m → 30 m	30 m resolution maps produced by applying the model to native 2 m resolution GAO reflectance imagery and resampling the resulting cover maps to 30 m;
Tanager 30 m:	30 m resolution maps produced by applying the model to native resolution Tanager reflectance imagery;
GAO 30 m + noise:	30 m resolution maps produced by applying the model to resampled GAO reflectance imagery with random noise added.

2.8. Field Validation

We used field estimates of live coral cover as validation for benthic mapping estimates from both sensors. As part of a larger campaign to validate GAO estimates across Hawai'i Island, we collected field estimates of live coral cover along the West Hawai'i coastline. From this validation set, 145 field estimates were within the Tanager-GAO comparison study region and could be used to compare model results between instruments and spatial resolutions. This collection included benthic data from 22 transects recorded June through August of 2023, and 123 photo interpretation plots recorded in July and August of 2024 (68 photos) and May of 2025 (55 photos).

Each transect was 25 m in length starting at a pre-defined random location and oriented along a random azimuth. A 0.25 m × 0.25 m quadrat (0.25 m^2) was moved along each transect and centered every 0.5 m [23]. At each quadrat position, the fractional cover of live coral, macroalgae, and sand was visually estimated. The average fractional cover of each class was estimated in 51 quadrat positions along each transect. Water depth of the starting point ranged from 3 to 15 m, while depth along the transects ranged from 1.5 m to 20 m.

For each photo interpretation plot, a camera mounted on a custom platform was positioned at a pre-selected random location such that the end of the lens was beneath the water surface. Captured images were processed and visually assessed by a single analyst to approximate the cover of live coral, macroalgae, and sand. Effort was made to derive estimates on a 5 m × 5 m area in the center of each image. A check assessment by two additional analysts indicated that uncertainty between analysts was minimal (SD = 0.1), and there was no evidence of bias by the main analyst. The depth range of the photo interpretation plots was 2 m to 20 m.

We compared the spline-adjusted model estimates of live coral cover for each benthic cover dataset against the above field-derived cover values. For each transect, a polygon feature was created that represented the transect line with a buffer of 2.5 m. Similarly, for each photo plot, a circular polygon feature with 5 m diameter was generated. For each of the four benthic cover datasets, pixels falling within each of these polygon features were averaged to obtain the model-estimated live coral cover for each Tanager scene and GAO flight line that overlapped with each polygon.

While the position and orientation of each transect was placed as close as possible to the specified values, transitioning from a position at the water surface to a location on the ocean floor vertically below the surface point is difficult in open water conditions, as is correctly orienting a transect along an azimuth. Similarly for the photo plots, while all effort was made to center the camera at the original specified location, actual photo locations were subject to GPS positional error, drifts from ocean current between initial positioning and camera capture, and errors due to lens orientations differing from vertical. For this reason, and the highly variable nature of coral cover on the landscape, we allowed for several iterations of positional shift of the polygons for each image and selected the local best match as validation pair for that polygon

and image combination. For 30 m images, this shift was allowed to be ±1 pixel (±30 m) in the x or y direction. For 2 m imagery this shift was allowed to be ±3 pixels (±6 m). For transects, the azimuth was allowed to vary by ±10°. We generated a scatterplot of the best match pairs of modeled cover and field-derived cover for each benthic cover dataset and used R^2 and root mean square error (RMSE) fit statistics to compare the represented instruments and spatial resolutions in as comparable an environment as possible.

2.9. Spatial Analysis

We used semivariograms to assess whether there were significant differences in the spatial patterns of the three benthic classes as estimated by the GAO and Tanager instruments. While we would normally average benthic estimates across GAO flight lines to obtain more stable results, doing so alters the variance structure in such a way that we could not compare it to Tanager estimates. Therefore, we computed semivariograms for each GAO flight line and averaged these across flight lines for a more direct comparison.

For each GAO flight line and for each benthic class, we computed the empirical variogram using the vario_estimate function from the gstools package version 1.7.0 [42] for the Python programming language (v. 3.12). This was done at the resampled 30 m resolution using lag distance bins with edges defined by boundaries at 30 m, 50 m, 75 m, 100 m, 150 m, 200 m, 300 m, 400 m, and 500 m. For each lag distance, we computed the average and standard deviation of the semivariance ($\hat{\gamma}$) values across flight lines. For comparison, we computed the empirical semivariograms for the benthic classes estimated from the single Tanager scene using the same lag distance bin boundaries.

3. Results

A comparison of spectral reflectance measured by the GAO and Tanager spectrometers over ocean indicated that both instruments produce similar spectra in the low-signal measurement environment of seawater (Figure 4). Reflectance peaked at just over 4% at around 485 nm and declined to about 1% at 400 nm. Reflectance values beyond 600 nm were less than 0.5%, making that spectral region unusable for benthic mapping. The low reflectance environment emphasizes the need for high signal-to-noise performance of imaging spectrometers for aquatic applications.

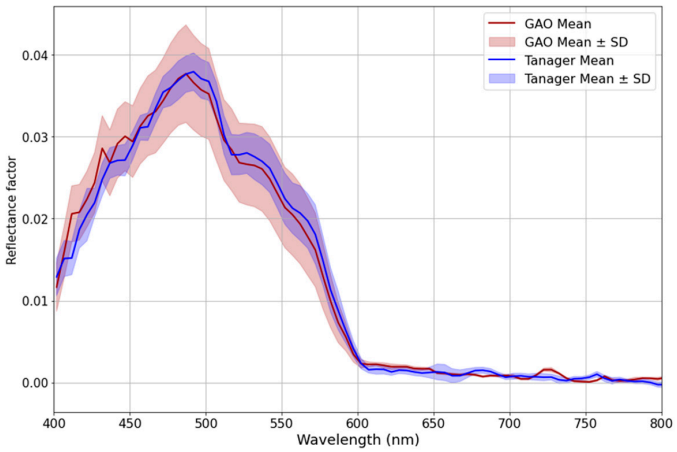


Figure 4. Comparison of GAO and Tanager measurements of remote sensing reflectance (R_{rs}) over reef after bias correction in the Tanager data and with glint removed. Mean values are shown with one standard deviation (SD) for an example area of 150 m × 150 m in the study region.

Despite these low reflectance conditions, coral cover maps from the 30 m Tanager and the resampled 30 m GAO flight lines captured similar spatial patterns among benthic

constituents (Figure 5). Areas of high and low coral cover, and gradations between highs and lows, were similar between the two datasets (Figure 5a,d). Sand and macroalgal fractions were also highly consistent between sensors (Figure 5b,c,e,f).

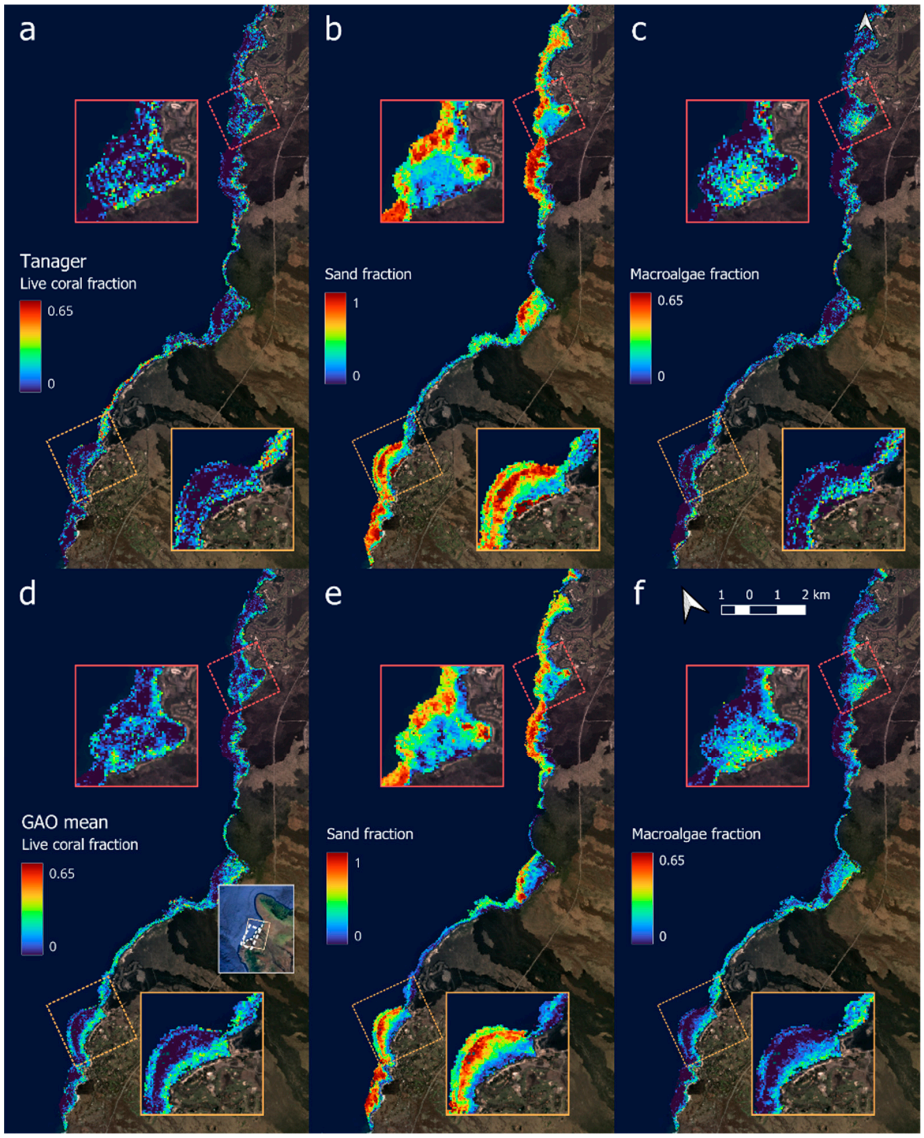


Figure 5. Benthic compositional mapping from (**a**–**c**) Tanager and (**d**–**f**) GAO imaging spectroscopy at 30 m resolution. The maps show the estimated fractional cover for the live coral, sand, and macroalgae benthic classes per 30 m pixel. Red and orange boxes are zoom images to reveal benthic compositional detail.

A key metric of reef condition—the live coral to macroalgal ratio (C:M)—was computed from the Tanager and GAO mapping results. The C:M ratio of all pixels in the Tanager data fell within the bounds of the C:M ratio of GAO flight line results (Figure 6). Kolmogorov–Smirnov tests on randomly selected sets of 500 coaligned pixels indicated no statistical difference between the mean distributions ($p > 0.70$).

Validation tests on the four benthic cover datasets showed how the two sensors compared to one another and how spatial resolution affected the results (Figure 7). The highest accuracy was achieved with the GAO 2 m imagery, with an $R^2 = 0.822$ and an RMSE = 0.097 (Figure 7a). Additional analysis of the GAO 2 m data indicated a much smaller RMSE for field transects (0.047) than for field photo interpretation plots (0.103), suggesting that transects are a more relatable estimator of benthic cover conditions relative to airborne imaging data.

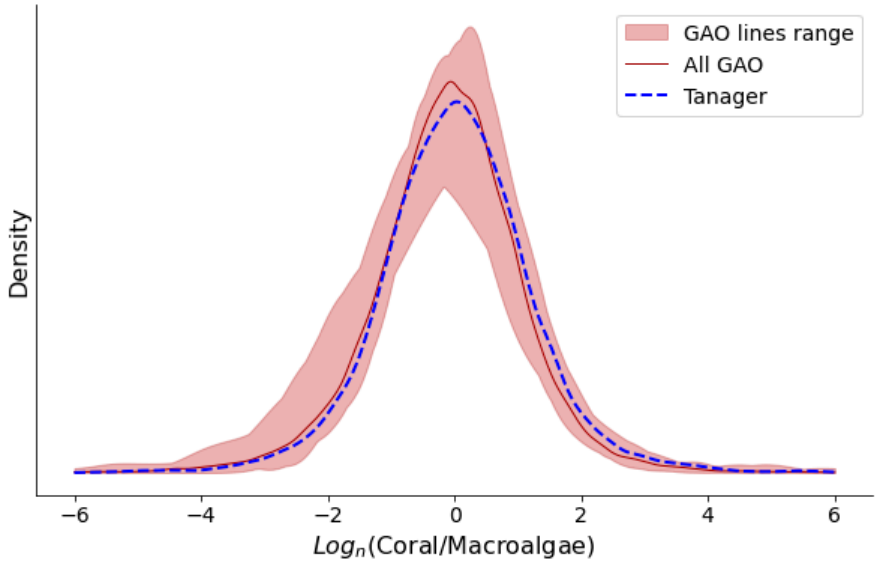


Figure 6. Histograms indicating the regional distribution of the ratio of live coral to macroalgal cover. Blue dashed line is the distribution from Tanager. Red line is the mean distribution from all GAO flight lines with the red shaded area indicating the variability in coral:macroalgal cover per flight line.

Downsampling the GAO 2 m benthic cover data to 30 m reduced the R^2 to 0.716 and RMSE to 0.113 (Figure 7b), showing that reduced spatial resolution has a significant negative effect on perceived accuracy when comparing large pixels to fine-scale field data. Importantly, rescaling the derived benthic cover maps from 2 m to 30 m greatly reduced the effect of noise because 225 individual 2 m pixels were averaged for each 30 m pixel, which advantaged to the GAO 2 m results over the GAO 30 m results. When the effect of noise on model results was generated, as in the Tanager 30 m dataset and the GAO 30 m + noise dataset, both achieved similar performance levels with an R^2 of 0.654 and 0.647, and similarly, a RMSE 0.107 and 0.109 for Tanager and GAO, respectively (Figure 7c,d).

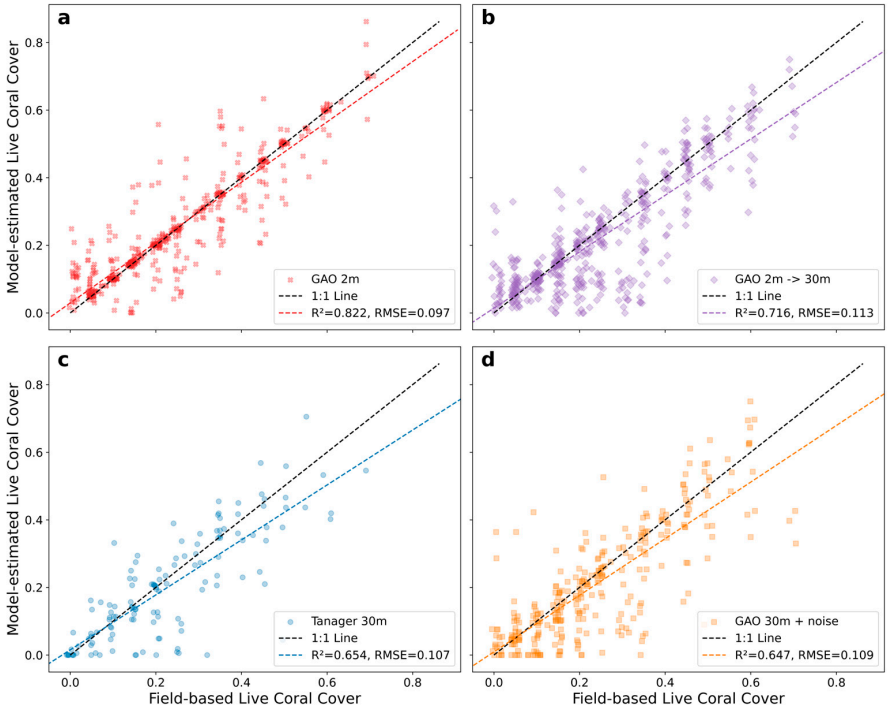


Figure 7. Field estimates of live coral cover (n = 145) compared to remotely estimated live coral cover from a single K-NN model applied to (**a**) GAO 2 m resolution reflectance data, (**b**) GAO 2 m resolution

reflectance data averaged to 30 m resolution, (**c**) Tanager 30 m reflectance data, and (**d**) resampled GAO 30 m reflectance data with simulated Tanager noise. Note that the field data were collected in bins of 5% (0.05) live coral cover.

A pixel-by-pixel comparison of Tanager and GAO benthic composition maps indicated broad geospatial agreement between the two data sources (Figure 8a–c). Most values of coaligned 30 m pixels were within 10% of one another, with notable exceptions in specific locations such as certain embayments and headland portions of the reef. Embayments are subject to temporal variability in turbidity caused by sediment loading [43], while headlands are subject to intermittent breaking waves. Despite these issues, the majority of the estimates from Tanager and GAO fell within the 95% confidence interval comparing Tanager to the variability of GAO results among all flight lines (Figure 8d–f).

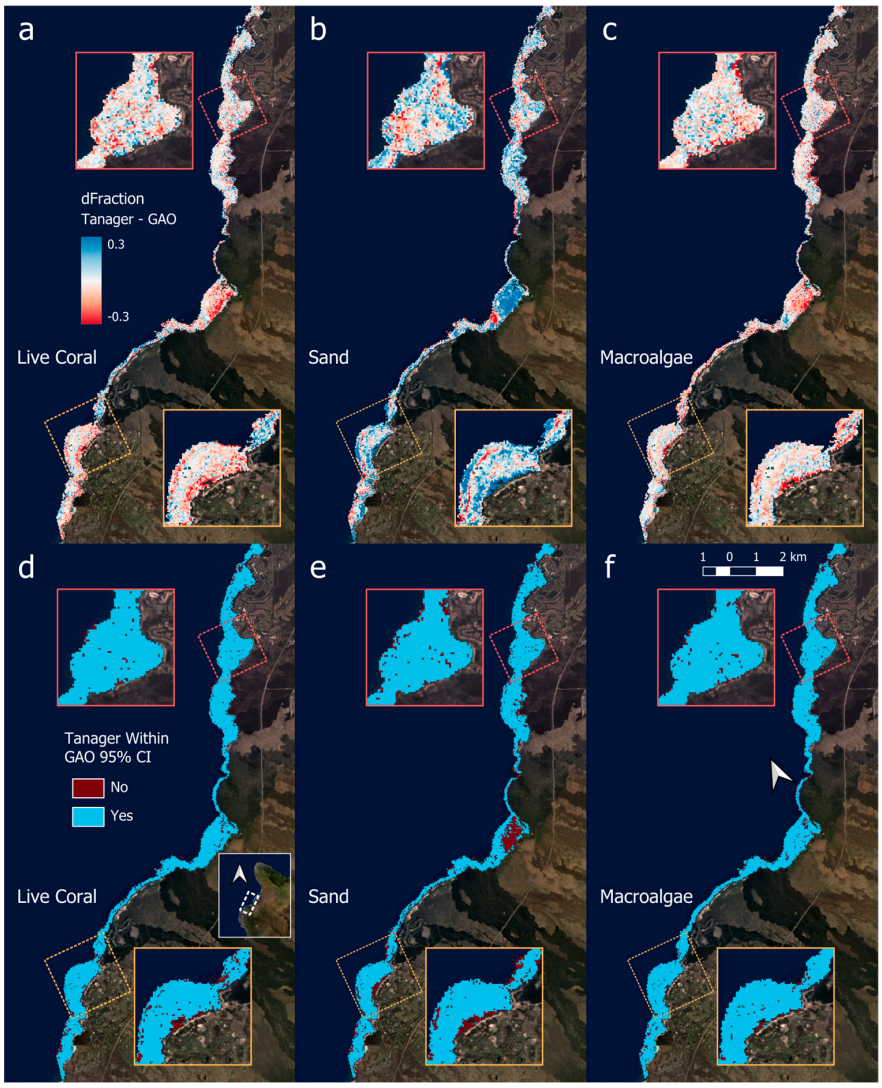


Figure 8. (**a**–**c**) Difference maps between the 30 m Tanager and GAO estimates of (**a**) live coral, (**b**) sand, and (**c**) macroalgae cover. (**d**–**f**) Maps depicting where Tanager estimates are within the 95% confidence intervals around the GAO mean estimates across all aircraft flight lines for (**d**) live coral, (**e**) sand, and (**f**) macroalgae classes. Maroon pixels represent pixels that outside the 95% confidence interval window and show locations where water turbidity was likely poor during the Tanager data collection. Red and orange boxes are zoom images to reveal detail in the difference between spaceborne and airborne results.

Semivariograms indicated the Tanager-based spatial structure of the reef was generally within the confidence range of the GAO results (Figure 9), indicating that spatial

relationships in scale of live coral, macroalgae, and sand cover variability across the study region were effectively captured in the Tanager imagery. One discrepancy was found for live coral cover, where the Tanager semivariance estimates were below the range of GAO for semivariogram lag distances less than 100 m. This finding indicated that there was generally more uniformity amongst neighboring (~3 pixels) coral cover estimates from Tanager than was found from GAO.

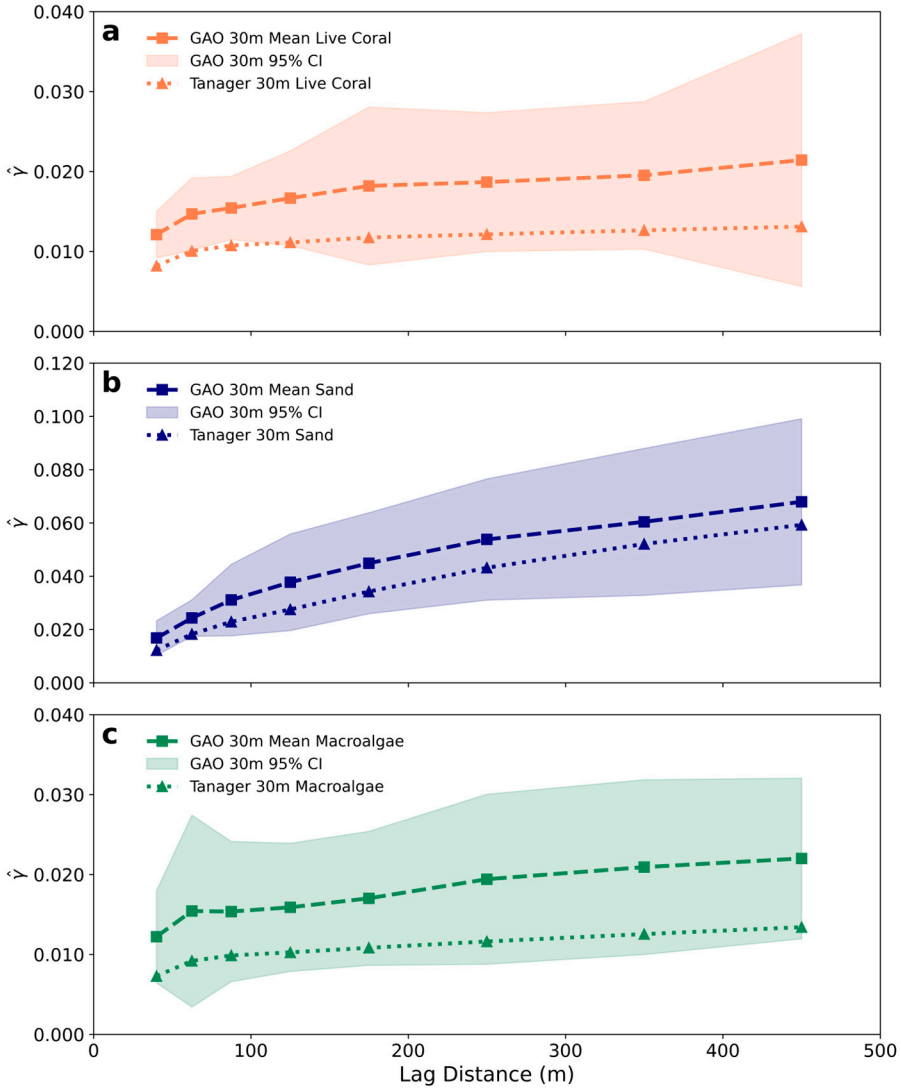


Figure 9. Semivariograms comparing estimates from 30 m GAO and Tanager imagery for (**a**) live coral, (**b**) sand, and (**c**) macroalgae benthic classes. The dashed lines indicate the mean semivariance estimates across all GAO flight lines at each lag distance. The dotted lines indicate the estimated semivariance from the single Tanager image. The shaded areas represent the 95% confidence interval from the 30 m GAO imagery for all flight lines.

4. Discussion

A comparison of Tanager and GAO imaging spectroscopy indicates that the two approaches yield equivalent local and regional estimates of live coral, macroalgal and sand cover to 25 m water depth in Hawai'i (Figure 5). Subregional areas of discrepancy between sensors coincide with known coastal conditions related to persistent ocean turbidity, such as from sediment flow into embayments, and breaking waves along coastal headlands (Figure 8). Importantly, there was no systematic bias in the Tanager results relative to the

GAO findings, and comparisons to field-based estimates of live coral cover were similar between the spaceborne and airborne observations.

The ratio of live coral to macroalgal cover (C:M) is a critical metric of reef condition [44,45], and it is listed as primary indicator of reef status by the International Coral Reef Initiative (https://icriforum.org/, accessed on 19 January 2026). The C:M ratio has become increasingly important as a multitemporal monitoring tool for reefs as they undergo stresses including heatwaves, storms, overfishing, pollution, and their combination. These stresses often favor the proliferation of macroalgae over coral, thereby altering the fundamental structure and functioning of reefs [43–45]. While repeat airborne imaging spectroscopy can technically provide multitemporal C:M monitoring, this has only been achieved at large scales once over the Hawaiian Islands, before and following the 2019 marine heatwave event [23]. Yet the financial cost of airborne monitoring remains high and the need for combining numerous flight lines, each containing different illumination, viewing and sea surface combinations, makes it challenging to operationalize over large areas and through time. This will be true with spaceborne approaches as well, given sufficiently large areas of monitoring that incorporate many satellite overpasses. However, fewer images, consistent sun-sensor geometry, and economy-of-scale effects favor the use of satellite observations, especially if the 30 m spatial resolution is sufficient for scientific, management, and conservation applications. Our study is the first to indicate that 30 m resolution spaceborne imaging spectroscopy from Tanager provides a reef-scale diagnostic C:M distribution similar to that derived from airborne imaging spectroscopy (Figure 6). Note that our C:M ratios cover a large range of values from <0.1 to >0.9, making the test broadly applicable. Similarly, the geospatial distributions of live coral, macroalgae, and sand were generally similar between Tanager and the GAO (Figures 4 and 8). Taken together, our findings suggest that Tanager imaging spectroscopy can provide reliable regional estimates of each benthic constituent and their ratios.

Coarsening the GAO data from its nominal spatial resolution of 2 m to 30 m for comparison to Tanager was not a trivial task. Incorporation of sensor noise, viewing and illumination geometry, and environmental conditions is key to generating a fair comparison. By doing so, we found that Tanager and GAO performed similarly overall. Moreover, Tanager appears to be robust for additional estimates of benthic macroalgal and sand cover, aligning geospatially with GAO estimates; however, we were unable to develop a formal validation of these two reef constituents. Future research should more carefully probe the accuracy and limits of macroalgae mapping as another key indicator of coral reef functioning and health.

A key issue in comparing live coral maps from multiple sensors, or even from the same sensor with data collected over time, rests in the selection of which model to use for spectroscopic analysis of ocean surface reflectance to derive estimates of benthic constituents. In our earlier work, we used deep learning models, which have become popular in the Earth Observation domain [46,47], to map live coral cover with high precision and accuracy from airborne imaging spectroscopy [23,24]. However, deep learning approaches often generate image data-specific results and can be difficult to transfer to new imaging sources. We addressed this issue by migrating our methods from deep learning to K-NN machine learning, which provided a more generalized set of model-based relationships between ocean surface reflectance and benthic constituent composition. Doing so led to a modest reduction in precision and accuracy at the GAO nominal resolution of 2 m. Specifically, with a deep learning approach we previously achieved higher precision and accuracy than achieved by the K-NN model used here (an R^2 of 0.94 and an RMSE of 0.08) [24]; In the present study, the K-NN approach yielded an R^2 of 0.82 and an RMSE of 0.09, respectively. However, this reduction was deemed acceptable in order to apply the same model to the

GAO and Tanager data at 30 m resolution. Doing so yielded an R^2 of 0.65 and a RMSE of 0.09, respectively, for both sensors. Importantly, this does not mean that the 30 m resolution simply lacks the precision and accuracy of the finer resolution model; Rather it indicates uncertainty in the placement of necessarily small field-based quadrat samples within large 30 m × 30 m image pixels. This idea is reinforced by the fact that simply averaging the 2 m coral cover estimates to 30 m resolution (GAO 2 m -> 30 m dataset) significantly reduced the R^2 and increased the RMSE over the 2 m model to 0.11, which is even slightly higher than the RMSE for both the GAO with noise and Tanger at 30 m resolution. Overall, we assess the field validation outcome as indicating sufficient performance in live coral mapping at 30 m resolution using Tanager.

Our findings strongly suggest that high-fidelity spaceborne imaging spectroscopy, such as from the Tanager satellite, can be used to generate synoptic maps that quantitatively capture the amount and spatial distribution of live coral cover over large areas. Until now, such an approach has only been operationalized by airborne imaging spectroscopy methods, while satellite-based estimates have been fewer and less quantitatively verified. Tanager carries a spectrometer of similar performance as the GAO and AVIRIS, thereby opening up new possibilities for taking live coral cover estimates to a global scale over time. Our work was affected by a brightness bias in the Tanager reflectance data due to apparent radiance calibration errors. Though we needed to remove this bias manually in this work, we do not believe this will be a continuing problem. Planet Labs PBC is continuing to improve radiance calibration techniques and should have this bias fixed in the future.

At this point in time, there is very little information on the total live coral cover of the world's reefs, and we know even less about changes in live coral cover or the ratio of live coral to macroalgal cover globally. While we know the extent of coral reefs like never before via the Allen Coral Atlas (https://allencoralatlas.org; accessed on 19 January 2026) [3], the composition of reefs in terms of living and dead coral, macroalgal cover, and other key indicators remains poorly understood. With an increasing number of spaceborne imaging spectrometers under development, a new era of coral reef mapping and monitoring will be made possible over time. Our results suggest that spaceborne spectroscopic methods will serve as a functional surrogate for airborne approaches at the resolutions achievable from low Earth orbit. A spatial resolution of 30 m appears sufficient for general mapping of live coral cover and change, which will greatly enhance and extend current benthic classification approaches. Repeatable global surveys of live coral will fuel new scientific, management, and restoration efforts at scale.

5. Conclusions

Assessment of live coral extent serves as a fundamental parameter for evaluating the composition, health and productivity of coral reefs. Despite operational estimates of benthic habitat extent achieved via satellite multispectral observations, the delineation of live coral from macroalgal cover has presented challenges attributed to signal attenuation caused by seawater, spectral similarity of benthic constituents, illumination and observation conditions, and more. Airborne imaging spectroscopy, exemplified by the capabilities of the Global Airborne Observatory (GAO), featuring high spectral resolution and signal-to-noise, has demonstrated operational proficiency in quantifying benthic constituents in low reflectance seawater environments, thereby facilitating accurate assessments of live coral cover. The advent of the Tanager satellite, equipped with a high-fidelity imaging spectrometer in low Earth orbit, presents a potential transition from airborne to spaceborne imaging spectroscopy for regional live coral detection and mapping. Through coordinated observations from Tanager and GAO, encompassing coral, macroalgal, and sand constituents at a spatial resolution of 30 m and to a depth of 25 m on a Hawaiian reef, both sensors exhibited

congruent spatial distributions of each benthic component. Specifically, Tanager yielded estimates of live coral cover comparable in precision and accuracy to those obtained from GAO. The proliferation of upcoming spaceborne imaging spectrometers, including those within the Tanager series, heralds a novel era in repeatable coral reef mapping, offering a solution for monitoring changes in coral populations at a global scale.

Author Contributions: Conceptualization, G.P.A. and A.R.; methodology, G.P.A., N.R.V., J.H. and K.L.R.; validation, G.P.A., N.R.V. and J.H.; formal analysis, N.R.V.; investigation, G.P.A., N.R.V., J.H. and K.L.R.; resources, G.P.A. and A.R.; data curation, N.R.V., J.H. and K.L.R.; writing—original draft preparation, G.P.A. and N.R.V.; writing—review and editing, G.P.A., N.R.V., J.H., K.L.R. and A.R.; visualization, N.R.V.; supervision, G.P.A.; project administration, G.P.A. and A.R.; funding acquisition, G.P.A. and A.R. All authors have read and agreed to the published version of the manuscript.

Funding: This collaborative study between the ASU Global Airborne Observatory and Planet Labs PBC was funded internally by each organization. The Global Airborne Observatory is made possible by support from private foundations, visionary individuals, and Arizona State University.

Data Availability Statement: Benthic composition maps and field data from Tanager-1 and the Global Airborne Observatory are available at https://doi.org/10.5281/zenodo.17943087 (accessed on 27 January 2026).

Conflicts of Interest: Authors Keely L. Roth and Amy Rosenthal were employed by the company Planet Labs PBC. The remaining authors declare that the research was conducted in the absence of any commercial or financial relationships that could be construed as a potential conflict of interest. The authors declare that this study received funding from Planet Labs PBC. The funder was not involved in the study design, collection, analysis, interpretation of data, the writing of this article or the decision to submit it for publication.

References

1. Andréfouët, S.; Muller-Karger, F.E.; Hochberg, E.J.; Hu, C.; Carder, K.L. Change Detection in Shallow Coral Reef Environments Using Landsat 7 ETM+ Data. *Remote Sens. Environ.* **2001**, *78*, 150–162. [CrossRef]
2. Asner, G.P.; Martin, R.E.; Mascaro, J. Coral Reef Atoll Assessment in the South China Sea Using Planet Dove Satellites. *Remote Sens. Ecol. Conserv.* **2017**, *3*, 57–65. [CrossRef]
3. Lyons, M.B.; Murray, N.J.; Kennedy, E.V.; Kovacs, E.M.; Castro-Sanguino, C.; Phinn, S.R.; Acevedo, R.B.; Alvarez, A.O.; Say, C.; Tudman, P.; et al. New Global Area Estimates for Coral Reefs from High-Resolution Mapping. *Cell Rep. Sustain.* **2024**, *1*, 100015. [CrossRef]
4. Mumby, P.J.; Edwards, A.J. Mapping Marine Environments with IKONOS Imagery: Enhanced Spatial Resolution Can Deliver Greater Thematic Accuracy. *Remote Sens. Environ.* **2002**, *82*, 248–257. [CrossRef]
5. Xu, H.; Liu, Z.; Zhu, J.; Lu, X.; Liu, Q. Classification of Coral Reef Benthos around Ganquan Island Using WorldView-2 Satellite Imagery. *J. Coast. Res.* **2019**, *93*, 466. [CrossRef]
6. Hedley, J.; Roelfsema, C.; Koetz, B.; Phinn, S. Capability of the Sentinel 2 Mission for Tropical Coral Reef Mapping and Coral Bleaching Detection. *Remote Sens. Environ.* **2012**, *120*, 145–155. [CrossRef]
7. Xu, J.; Zhao, J.; Wang, F.; Chen, Y.; Lee, Z. Detection of Coral Reef Bleaching Based on Sentinel-2 Multi-Temporal Imagery: Simulation and Case Study. *Front. Mar. Sci.* **2021**, *8*, 584263. [CrossRef]
8. Kabiri, K.; Rezai, H.; Moradi, M. Mapping of the Corals around Hendorabi Island (Persian Gulf), Using WorldView-2 Standard Imagery Coupled with Field Observations. *Mar. Pollut. Bull.* **2018**, *129*, 266–274. [CrossRef]
9. Nguyen, T.; Liquet, B.; Mengersen, K.; Sous, D. Mapping of Coral Reefs with Multispectral Satellites: A Review of Recent Papers. *Remote Sens.* **2021**, *13*, 4470. [CrossRef]
10. Zuo, X.; Su, F.; Zhang, J.; Wu, W. Using Landsat Data to Detect Change in Live to Recently (<6 Months) Dead Coral Cover in the Western Xisha Islands, South China Sea. *Sustainability* **2020**, *12*, 5237. [CrossRef]
11. Newman, C.M. Assessing the Effect of Management Zonation on Live Coral Cover Using Multi-Date IKONOS Satellite Imagery. *J. Appl. Remote Sens.* **2007**, *1*, 011504. [CrossRef]
12. Hedley, J.D.; Mumby, P.J. Biological and Remote Sensing Perspectives of Pigmentation in Coral Reef Organisms. *Adv. Mar. Biol.* **2002**, *43*, 277–317. [CrossRef]

13. Joyce, K.E.; Phinn, S.R.; Roelfsema, C.M.; Neil, D.T.; Dennison, W.C. Combining Landsat ETM+ and Reef Check Classifications for Mapping Coral Reefs: A Critical Assessment from the Southern Great Barrier Reef, Australia. *Coral Reefs* **2004**, *23*, 21–25. [CrossRef]
14. Hedley, J.D.; Roelfsema, C.M.; Chollett, I.; Harborne, A.R.; Heron, S.F.; Weeks, S.J.; Skirving, W.J.; Strong, A.E.; Eakin, C.M.; Christensen, T.R. Remote Sensing of Coral Reefs for Monitoring and Management: A Review. *Remote Sens.* **2016**, *8*, 118. [CrossRef]
15. Li, J.; Fabina, N.S.; Knapp, D.E.; Asner, G.P. The Sensitivity of Multi-Spectral Satellite Sensors to Benthic Habitat Change. *Remote Sens.* **2020**, *12*, 532. [CrossRef]
16. Hochberg, E.J.; Atkinson, M.J. Spectral Discrimination of Coral Reef Benthic Communities. *Coral Reefs* **2000**, *19*, 164–171. [CrossRef]
17. Eakin, C.M.; Lough, J.M.; Heron, S.F. *Climate Variability and Change: Monitoring Data and Evidence for Increased Coral Bleaching Stress*; Springer International Publishing: Cham, Switzerland, 2009; pp. 41–67.
18. Kennedy, E.V.; Roelfsema, C.M.; Lyons, M.B.; Kovacs, E.M.; Borrego-Acevedo, R.; Roe, M.; Phinn, S.R.; Larsen, K.; Murray, N.J.; Yuwono, D.; et al. Reef Cover, a Coral Reef Classification for Global Habitat Mapping from Remote Sensing. *Sci. Data* **2021**, *8*, 196. [CrossRef] [PubMed]
19. Joyce, K.E.; Phinn, S.R. Spectral Index Development for Mapping Live Coral Cover. *J. Appl. Remote Sens.* **2013**, *7*, 073590. [CrossRef]
20. Leiper, I.; Phinn, S.; Roelfsema, C.; Joyce, K.; Dekker, A. Mapping Coral Reef Benthos, Substrates, and Bathymetry, Using Compact Airborne Spectrographic Imager (CASI) Data. *Remote Sens.* **2014**, *6*, 6423–6445. [CrossRef]
21. Thompson, D.R.; Hochberg, E.J.; Asner, G.P.; Green, R.O.; Knapp, D.E.; Gao, B.-C.; Garcia, R.; Gierach, M.; Lee, Z.; Maritorena, S. Airborne Mapping of Benthic Reflectance Spectra with Bayesian Linear Mixtures. *Remote Sens. Environ.* **2017**, *200*, 18–30. [CrossRef]
22. Asner, G.P.; Knapp, D.E.; Boardman, J.; Green, R.O.; Kennedy-Bowdoin, T.; Eastwood, M.; Martin, R.E.; Anderson, C.; Field, C.B. Carnegie Airborne Observatory-2: Increasing Science Data Dimensionality via High-Fidelity Multi-Sensor Fusion. *Remote Sens. Environ.* **2012**, *124*, 454–465. [CrossRef]
23. Asner, G.P.; Vaughn, N.R.; Martin, R.E.; Foo, S.A.; Heckler, J.; Neilson, B.J.; Gove, J.M. Mapped Coral Mortality and Refugia in an Archipelago-Scale Marine Heat Wave. *Proc. Natl. Acad. Sci. USA* **2022**, *119*, e2123331119. [CrossRef] [PubMed]
24. Asner, G.P.; Vaughn, N.R.; Heckler, J.; Knapp, D.E.; Balzotti, C.; Shafron, E.; Martin, R.E.; Neilson, B.J.; Gove, J.M. Large-Scale Mapping of Live Corals to Guide Reef Conservation. *Proc. Natl. Acad. Sci. USA* **2020**, *117*, 33711–33718. [CrossRef]
25. Parsons, M.; Bratanov, D.; Gaston, K.J.; Gonzalez, F. UAVs, Hyperspectral Remote Sensing, and Machine Learning Revolutionizing Reef Monitoring. *Sensors* **2018**, *18*, 2026. [CrossRef]
26. Mills, M.S.; Ungermann, M.; Rigot, G.; Den Haan, J.; Leon, J.X.; Schils, T. Assessment of the Utility of Underwater Hyperspectral Imaging for Surveying and Monitoring Coral Reef Ecosystems. *Sci. Rep.* **2023**, *13*, 21103. [CrossRef]
27. Kutser, T.; Miller, I.; Jupp, D.L.B. Mapping Coral Reef Benthic Substrates Using Hyperspectral Space-Borne Images and Spectral Libraries. *Estuar. Coast. Shelf Sci.* **2006**, *70*, 449–460. [CrossRef]
28. Duren, R.; Cusworth, D.; Ayasse, A.; Howell, K.; Diamond, A.; Scarpelli, T.; Kim, J.; O'neill, K.; Lai-Norling, J.; Thorpe, A.; et al. The Carbon Mapper Emissions Monitoring System. *Atmos. Meas. Tech.* **2025**, *18*, 6933–6958. [CrossRef]
29. Asner, G.P.; Vaughn, N.; Heckler, J. *Global Airborne Observatory: Hawaiian Islands Live Coral Cover in 2019*; Zenodo: Geneva, Switzerland, 2020.
30. Thompson, D.R.; Natraj, V.; Green, R.O.; Helmlinger, M.C.; Gao, B.-C.; Eastwood, M.L. Optimal Estimation for Imaging Spectrometer Atmospheric Correction. *Remote Sens. Environ.* **2018**, *216*, 355–373. [CrossRef]
31. Brodrick, P.G.; Thompson, D.R.; Bohn, N.; Carmon, N.; Eckert, R.; Montgomery, J.; Wurster, K.; Vaughn, N.; Greenberg, E. *Isofit*; Zenodo: Geneva, Switzerland, 2025.
32. Green, R.O.; Thompson, D.R. An Earth Science Imaging Spectroscopy Mission: The Earth Surface Mineral Dust Source Investigation (EMIT). In Proceedings of the IGARSS 2020—2020 IEEE International Geoscience and Remote Sensing Symposium, Waikoloa, HI, USA, 26 September–2 October 2020; IEEE: Piscataway, NJ, USA, 2020; pp. 6262–6265.
33. Brodrick, P.G.; Carmon, N. *Arth Surface Mineral Dust Source Investigation (EMIT) Level 2A Data Product User Guide*; Jet Propulsion Laboratory, California Institute of Technology: Pasadena, CA, USA, 2022; p. 17.
34. European Space Agency. *Airbus Copernicus DEM*; European Space Agency: Paris, France, 2022.
35. Hondula, K.L.; König, M.; Grunert, B.K.; Vaughn, N.R.; Martin, R.E.; Dai, J.; Jamalinia, E.; Asner, G.P. Mapping Water Quality in Nearshore Reef Environments Using Airborne Imaging Spectroscopy. *Remote Sens.* **2024**, *16*, 1845. [CrossRef]
36. König, M.; Hondula, K.; Noel, P.; Nick, V.; Asner, G. *CMLandOcean/Bio_optics: V0.0.2*; Zenodo: Geneva, Switzerland, 2024.
37. Gege, P.; Groetsch, P. *A Spectral Model for Correcting Sun Glint and Sky Glint*; Optica Publishing Group: Washington, DC, USA, 2016.
38. Feyisa, G.L.; Meilby, H.; Fensholt, R.; Proud, S.R. Automated Water Extraction Index: A New Technique for Surface Water Mapping Using Landsat Imagery. *Remote Sens. Environ.* **2014**, *140*, 23–35. [CrossRef]

39. Xu, H. Modification of Normalised Difference Water Index (NDWI) to Enhance Open Water Features in Remotely Sensed Imagery. *Int. J. Remote Sens.* **2006**, *27*, 3025–3033. [CrossRef]
40. Albert, A.; Mobley, C. An Analytical Model for Subsurface Irradiance and Remote Sensing Reflectance in Deep and Shallow Case-2 Waters. *Opt. Express* **2003**, *11*, 2873. [CrossRef]
41. Gege, P. The Water Color Simulator WASI: An Integrating Software Tool for Analysis and Simulation of Optical in Situ Spectra. *Comput. Geosci.* **2004**, *30*, 523–532. [CrossRef]
42. Müller, S.; Schüler, L.; Zech, A.; Heße, F. GSTools v1.3: A Toolbox for Geostatistical Modelling in Python. *Geosci. Model Dev.* **2022**, *15*, 3161–3182. [CrossRef]
43. Gove, J.M.; Williams, G.J.; Lecky, J.; Brown, E.; Conklin, E.; Counsell, C.; Davis, G.; Donovan, M.K.; Falinski, K.; Kramer, L.; et al. Coral Reefs Benefit from Reduced Land–Sea Impacts under Ocean Warming. *Nature* **2023**, *621*, 536–542. [CrossRef]
44. Bruno, J.F.; Precht, W.F.; Vroom, P.S.; Aronson, R.B. Coral Reef Baselines: How Much Macroalgae Is Natural? *Mar. Pollut. Bull.* **2014**, *80*, 24–29. [CrossRef] [PubMed]
45. McManus, J.W.; Polsenberg, J.F. Coral–Algal Phase Shifts on Coral Reefs: Ecological and Environmental Aspects. *Prog. Oceanogr.* **2004**, *60*, 263–279. [CrossRef]
46. Persello, C.; Wegner, J.D.; Hansch, R.; Tuia, D.; Ghamisi, P.; Koeva, M.; Camps-Valls, G. Deep Learning and Earth Observation to Support the Sustainable Development Goals: Current Approaches, Open Challenges, and Future Opportunities. *IEEE Geosci. Remote Sens. Mag.* **2022**, *10*, 172–200. [CrossRef]
47. Schmitt, M.; Ahmadi, S.A.; Xu, Y.; Taşkin, G.; Verma, U.; Sica, F.; Hänsch, R. There Are No Data Like More Data: Datasets for Deep Learning in Earth Observation. *IEEE Geosci. Remote Sens. Mag.* **2023**, *11*, 63–97. [CrossRef]

Disclaimer/Publisher's Note: The statements, opinions and data contained in all publications are solely those of the individual author(s) and contributor(s) and not of MDPI and/or the editor(s). MDPI and/or the editor(s) disclaim responsibility for any injury to people or property resulting from any ideas, methods, instructions or products referred to in the content.